sciendo

POLISH MARITIME RESEARCH 4 (104) 2019 Vol. 26; pp. 134-141
10.2478/pomr-2019-0075

BLADE SECTION PROFILE ARRAY LIFTING SURFACE DESIGN METHOD FOR MARINE SCREW PROPELLER BLADE

Przemysław Król
Ship Design and Research Centre, Gdańsk, Poland
Gdańsk University of Technology, Poland

ABSTRACT

The lifting surface model is widely used in screw propeller design and analysis applications. It serves as a reliable tool for determination of the propeller blade mean line and pitch distribution. The main idea of this application was to determine the blade shape that would satisfy the kinematic boundary condition on its surface with the prescribed bound circulation distribution over it. In this paper a simplified lifting surface method is presented – in which the 3D task for the entire blade is replaced by a set of 2D tasks for subsequent blade section profiles.

Keywords: marine propeller, lifting surface, blade section profile, design

INTRODUCTION

A very common basis for designing a marine propeller blade is the lifting line model, replacing the propeller blade with a concentrated radial bound vortex having variable circulation and adequate vortex wake. In most cases, a real marine propeller blade sharply deviates from such simplification due to the finite chord length, possibly non-symmetrical outline etc. Because of that, a decision on the pitch and camber distribution that satisfies the dynamic requirements for the propeller cannot be done within the frame of the lifting line model alone. This was the reason for the elaboration of numerous lifting surface approaches. The first attempts were quite simple and rather rudimentary – mainly due to the limitations of available computational resources [5]. Moreover, these were applied mainly in the form of pre-calculated correction factors, interpolated in dependency on the main parameters of the designed propellers. One widely known model of this kind was elaborated by Ludweig and Ginzel. Formally, it was limited to three-bladed propellers with a symmetrical outline and elliptical loading distribution. Despite substantial simplifications, their model was widely used in the 1950s and early 1960s – however, recent analysis has revealed that in many cases the designed propellers were hydrodynamically overloaded.

A much more developed model was utilised by Morgan, Silovic and Denny [14] and was widely used for a long time. Even nowadays, "orthodox" propeller designs may be successfully obtained using it.

However, from a theoretical point of view, the best approach is to determine the pitch and camber distribution individually for each particular case. A solution for such task was given by Greeley and Kerwin [4]. They used a simplified vortex wake treatment and algorithm of blade shape determination involving vector operations on the local velocity field, but certain stability problems occurred. However, the model allowed them to elaborate successful designs of propeller blades and stimulated other researchers to pursue better propeller designs through the use of vortex models [3, 10]. Preparing a correct propeller design is especially important nowadays in the present era of increased awareness of the ecological problems connected with greenhouse gas emissions [19].

Although current vortex methods are being displaced by modern RANSE-based codes [15, 16], these still prove to be of interest to researchers [1, 3, 12]. Even for complicated system geometry, they are capable of solving practical technical problems [8, 13].

In the paper, the author's approach for utilising the lifting surface model in propeller design is presented. The main

idea is to replace the three-dimensional design problem for marine propeller blades with an array of two-dimensional problems solved for blade section profiles.

DESIGN ALGORITHM

BLADE SECTION PROFILE DESIGN

The basis for further work presented in this paper is the design algorithm, dedicated to two-dimensional blade section profiles. The main idea is to determine the mean line shape and angle of attack that would satisfy the kinematic boundary condition for the prescribed circulation distribution over the camber surface, representing the profile. The input data that has to be specified is the set of lift force coefficients corresponding to the required lift generated by the particular profile at design conditions. The loading distribution over the profile chord is also freely decided by the designer, as long as zero loading is preserved at the trailing edge. The most basic and well recognised ones are "roof-top" NACA a = 0.8 and elliptical distributions, but the possible applications are obviously not limited to these two. It is, however, to be underlined that convergent geometry could be obtained for NACA a = 1.0, which has a constant loading distribution from the leading to the trailing edge, but this would not meet its assumed parameters in real fluid, due to ignoring the Kutta condition.

The designer has to specify the thickness of the profile. Limitations arise from the source-sink representation of thickness effects, which makes it necessary to apply a zero thickness value at the trailing edge, to preserve the mass-conservation in the flow.

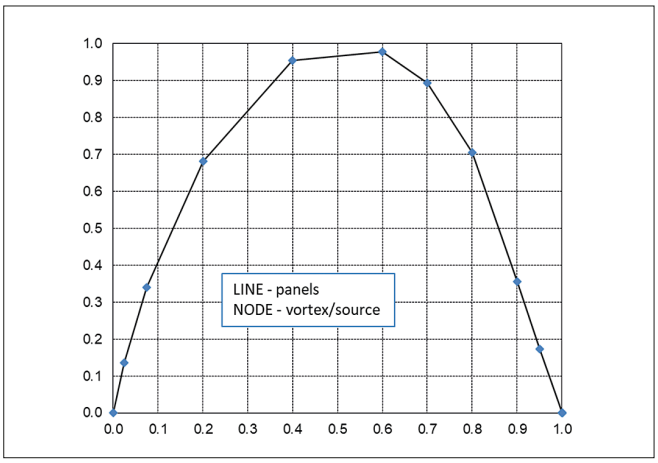

Fig. 1. Discrete lifting surface grid for profile design (different scales on x and y axis)

With a simple rearrangement of the well-known Zhoukovsky equation, the relation between the total bound circulation of the profile and the required lift force coefficient may be found:

$$\Gamma = \frac{1}{2} c U_0 C_L \tag{1}$$

where c is the profile chord length and U_0 is the external flow speed in which the profile operates. The bound circulation Γ is distributed along the profile continuously, generating local circulation density γ:

$$\gamma = \frac{\partial \Gamma}{\partial c} \tag{2}$$

The function describing the chordwise distribution of circulation density γ depends on the selected loading distribution. In the numerical application, discrete vortices are used instead of a continuous circulation distribution. If the blade section is described with a grid consisting of N straight line segments (these are spaced over the mean line), then the circulation of the particular discrete vortex is given as:

$$\Gamma_i = c \int_i^{i+1} \gamma dx_c \tag{3}$$

where i is the index referring to the subsequent discrete element of the vortex grid and x_c is a dimensionless chord fraction. At the same points as the vortices, the sources are placed also, to represent thickness effects. Their intensity is given as:

$$Q_i = U_0 (t_{i+1} - t_i) \tag{4}$$

where t_i is the profile thickness at the corresponding x_{c_i} chordwise position. When both the vortices circulations and the sources intensities are known, induced velocities may be easily found at each point over the profile. Summing them with the external velocity gives the total velocity field, which is used for determination of the blade section shape:

$$y = c \int_{LE}^{TE} \frac{U_y}{U_x} dx_c \tag{5}$$

where U_x and U_y are the total velocities in the x and y directions respectively, at the considered point.

As all the calculations are conducted for dimensionless parameters, the external velocity has a prescribed value equal to V = 1 m/s in the x direction. After determination of the blade section coordinates, the calculations may be repeated – as the singularities positions will update respectively. This leads to an updated velocity field, of course, which will result in a slightly different profile form. This loop converges quite swiftly, under approx. 10 times for moderately loaded profiles. When the geometry solution has converged, the angle of attack value is calculated as the one between the external velocity (practically: the x axis) and a straight line connecting the first and last singularity over the mean line. Accordingly, mean line offsets are determined as the distance between the abovementioned straight line and the respective point on the mean line.

The algorithm described above was applied to a design blade section with a lift force coefficient equal to C_L = 0.20 with NACA a = 0.8 loading distribution. Fig. 2 gives the comparison between the designed mean line and tabular one [5]:

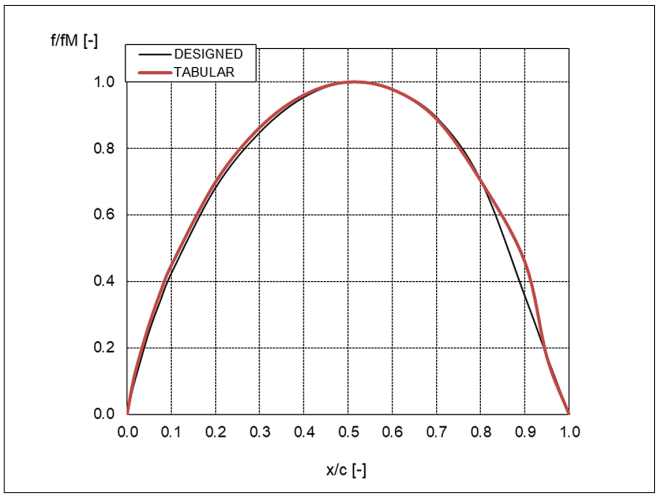

Fig. 2. Mean line designed for NACA a = 0.8 loading distribution and tabular mean line NACA a = 0.8 (different scales on x and y axis)

PROPELLER BLADE DESIGN

In the previous paragraph a blade section placed in two-dimensional flow was considered. The flow conditions over the marine screw propeller are substantially different from that, and three-dimensionality has to be included in the analysis. It was, however, possible to successfully replace the three-dimensional design task for a screw propeller blade with an array of sub-tasks of designing two-dimensional blade section profiles.

The initial part of the propeller blade design is to determine the radial bound circulation distribution that would satisfy the delivered thrust / consumed power requirements for the propeller, to decide the blade outline etc. This can be done with any of the well-known algorithms [5, 6], so it is not a subject of consideration here. The part of the design algorithm which is focused on starts from the determination of the pitch and camber distributions. Consequently, it has been assumed that all the necessary data, especially the radial bound circulation distribution and local values of induced advance angles, are known. What the designer has to decide are – similarly to the case of blade section profile design – the chordwise loading and thickness distributions.

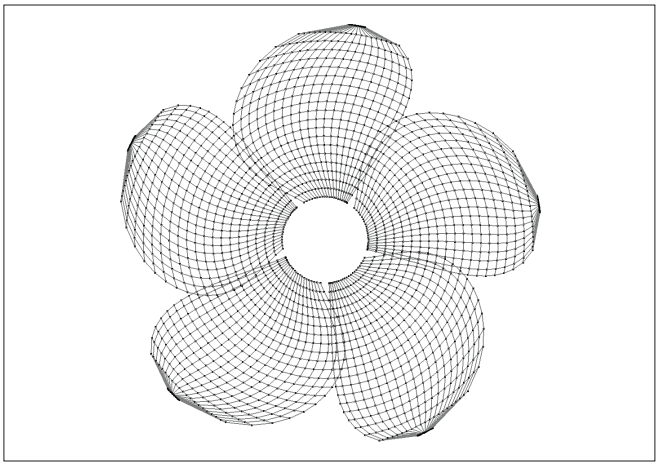

Fig. 3. Discrete lifting surface grid for propeller design

In the first step, the induced velocities at each panel middle-point are calculated to obtain the total velocity at each of these. Subsequently, it is summed with the external velocity – consisting of the axial speed in non-uniform inflow and the tangential one resulting from propeller rotation:

$$U_{\text{total}} = V(1 - w_{\text{r}}) + \omega \times r + u_{\text{ind}} \tag{6}$$

where w_{r} is the average wake fraction coefficient at the respective radius, and u ind is the local induced velocity vector. The induced velocity vector is the sum of the vortex and source line elements. Vortex-induced velocities are obtained by means of the Biot–Savart law. Source line elements are replaced with point sources in such number that the distance between each source element is at least 5 times smaller than the distance between the point source and a calculation point [18].

After calculating the total velocity vector for each point, it is divided into axial and tangential components. In further calculations, these are treated as components of the two-dimensional velocity field, which allows the blade section profile algorithm to be applied directly. The radial component of velocity is neglected; however, this simplification turned out to be justified by the agreement obtained between the design input values and corresponding ones determined during towing tank tests with the designed propeller. This will be considered in a further part of the text.

Similarly to the case of a two-dimensional blade section, obtaining the blade geometry is an iterative process. In the case adopted for practical application, 6 iterations were enough to receive a convergent solution. The applied vortex grid was a uniform one, with 20 x 20 radial x chordwise vortex segments. The first attempt was to use non-uniform mesh, which was denser towards the blade tip. As a result, it turned out to generate a blade with a very small pitch ratio (around 0.25 of mean value) and very high camber in the tip region.

The outer radii pitch angles may be smaller than the induced advance angles calculated with the lifting line method at respective positions, specifically for the lifting surface method. This effect is known in the literature and increases with the increasing propeller expanded area ratio and blades skew. The effect is weaker for warped propellers compared with non-balanced skew-induced rake propellers [2].

INFLUENCE OF VORTEX WAKE

The possibility of including the influence of the vortex wake directly instead of using a simplified lifting line is the significant advantage of the lifting surface algorithm. First of all, using a discrete representation of the vortex wake allows an iterative relaxation algorithm to be applied, like the one described in [9] or [11] to determine its geometry adequate to the particular case. Also, experimental data on wake geometry as described in [17] may then be utilised even at this stage of blade design.

The initial guess for the vortex wake shape is a variable pitch helical surface, where the pitch angle at each radius is taken as equal to the induced advance angle coming from preceding lifting line calculations. In this "zero-iteration" propeller, slipstream contraction is neglected. Fig. 4 presents two blade pitch distributions – one determined at the vortex wake left as in the initial guess, and the second determined for iteratively relaxed wake. It has to be underlined that, as the induced velocities depend not only on the singularities strength but also on their position, the wake relaxation has to be repeated after each iterative update of the blade geometry.

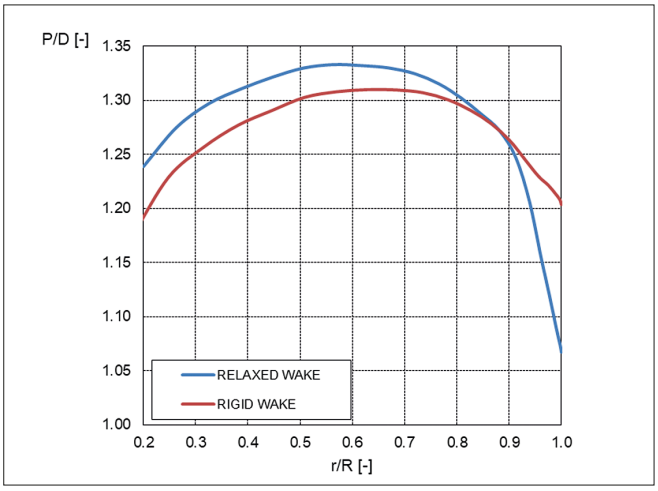

Fig. 4. Influence of vortex wake on blade's pitch

It can be easily seen that applying relaxed wake resulted in significant tip unloading with respect to the rigid wake calculations with a parallel increase in loading over the remaining part of the blade.

EXPERIMENTAL VALIDATION

Using the method described above, two propellers were designed for the Kriso Container Ship (KCS). Their models were manufactured and tested in the Ship Hydromechanics Division of CTO. The numbers of these propeller models are P759 and P766. The first one was designed with a half-mature version of the design software, implementing the methods described above. Moreover, it was not designed as a wake-adapted propeller but for an entirely averaged velocity field, so it is effectively designed as an open-water propeller. Accordingly, propeller P766 was designed with a complete version of the software as a wake-adapted one.

The design assumptions for these propellers were taken as follows: diameter D = 7900 mm, number of blades Z = 5, ship speed V_S = 24.0 knots, rate of revolution n = 80.00 rpm. For propeller P759 the required thrust force was taken as T = 2121 kN. After conducting a self-propulsion test with this propeller, a new value of the thrust deduction factor t was available and hence a required thrust of T = 2134 kN was adopted for the design of P766. The propellers differ in the frame of the expanded area ratio, which was EAR = 0.896 for P759 and EAR = 1.029 for P766. The differences result from a cavitation analysis that showed that a notably higher EAR value was required to limit the cavitation phenomena on the final propeller. This was not considered in detail in the case of P759 as it is in fact designed as an open-water propeller and hence, by definition, was not expected to operate free of cavitation. The pitch ratio at dimensionless radius r/R = 0.7 is equal to $P_{0.7}/D$ = 1.320 in the case of propeller P759 and $P_{0.7}/D$ = 1.327 for propeller P766. Fig. 6 presents the pitch and camber distributions of both propellers.

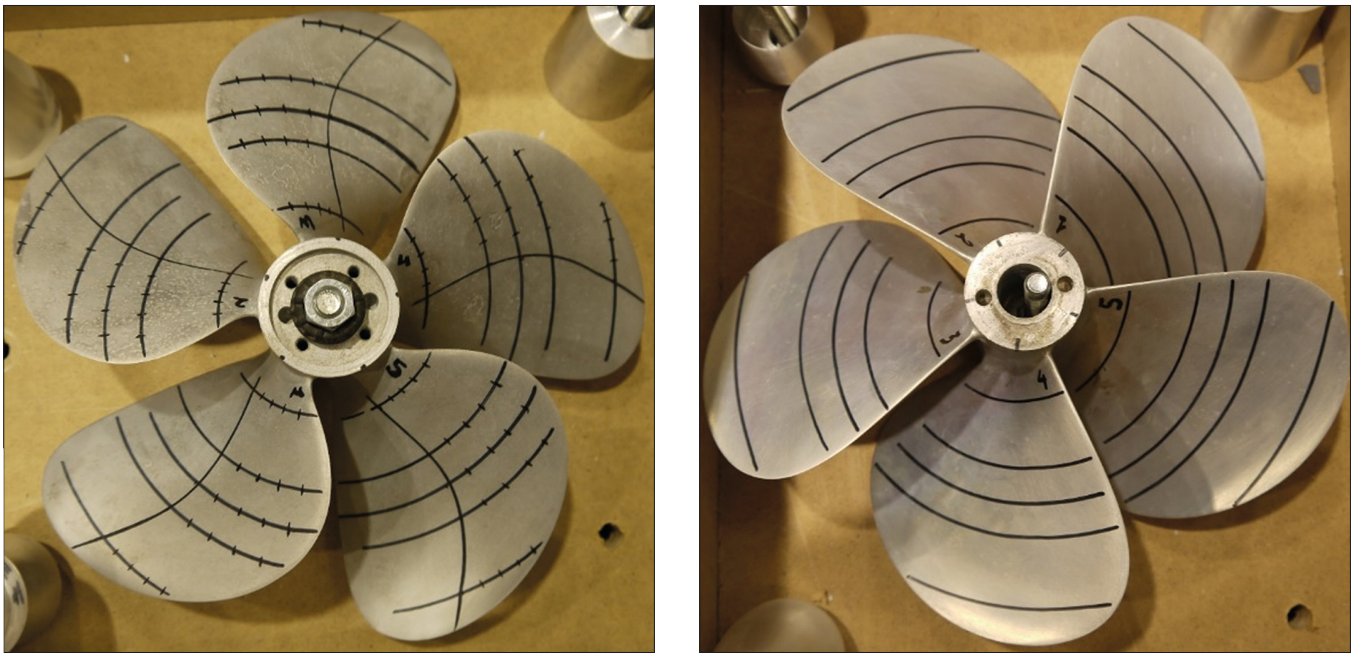

Fig. 5. Propeller model P759, suction side (left) and propeller model P766, pressure side (right)

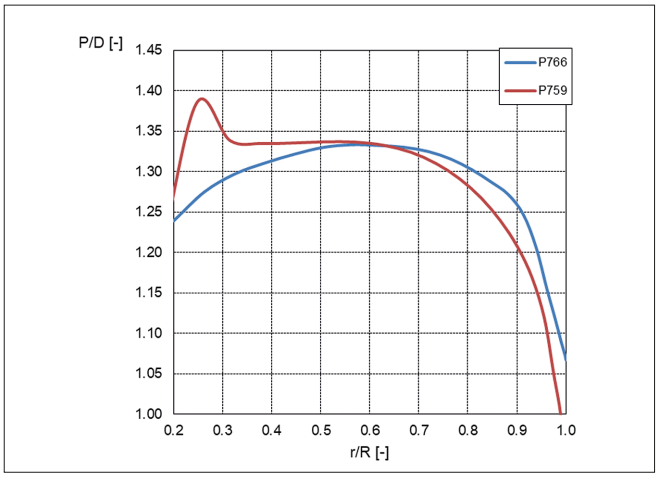

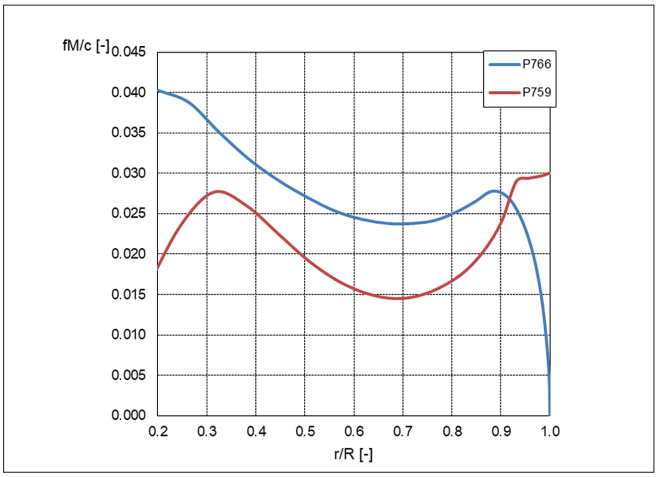

Fig. 6. Designed propellers pitch (left) and camber (right) distributions

In the case of both propellers, the camber ratio for radii above 0.90 was reduced to below the theoretical values for technological reasons. The reduction was much more robust in the case of the P759 propeller, which resulted in a discontinuous camber distribution above radius 0.90 for it. A purely theoretical camber distribution would notably increase in the tip region, which would lead to an unnatural spoon-like shape of the tip. Analytical calculations conducted with the lifting surface model confirmed that reducing the tip camber did not influence the propellers' hydrodynamic properties significantly.

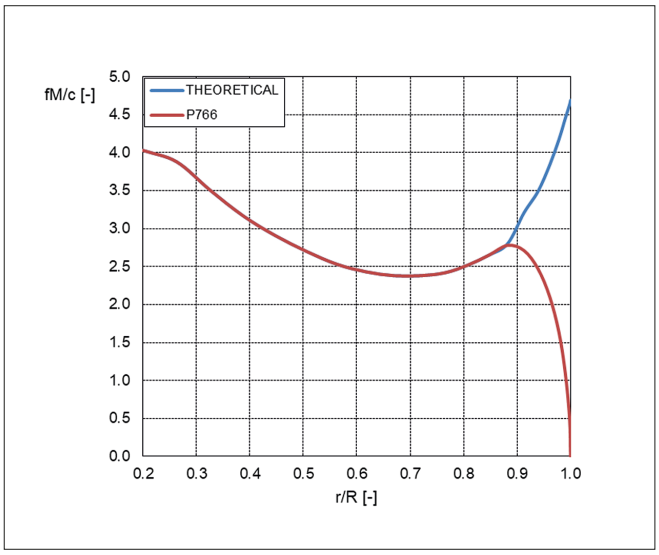

Fig. 7. Theoretical and applied camber, propeller P766

Fig. 7 gives the comparison between the theoretical camber distribution and the one adopted for propeller P766 design:

Fig. 8 gives the dimensional mean line ordinates vs. the non-dimensional chord fractions of selected profiles – after the first iteration and after the final iteration adopted for the propeller P766 design respectively. The presented mean lines are given after tip camber reduction. The initial guess for the mean line is a non-cambered flat profile so it is not presented here.

The main differences between the shapes of the mean lines are concentrated in the vicinity of the trailing edge. At the beginning of the iteration process, this region reveals a discontinuity of the mean line shape, but this disappears swiftly. It can be seen also that the maximum camber is slightly lower for the outer radii in the case of the final geometry.

The radial distributions of the design operation parameters for both propellers are given in Figs. 9–12.

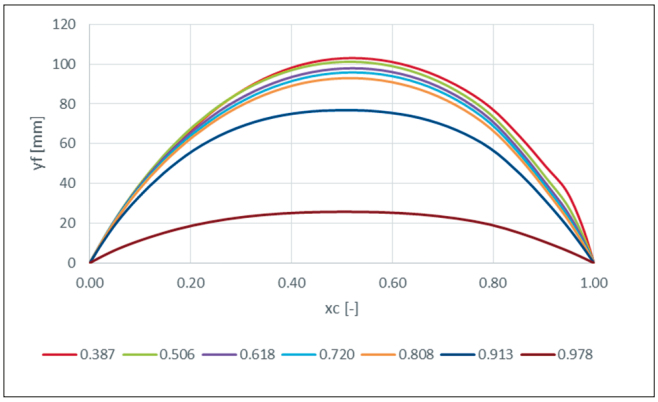

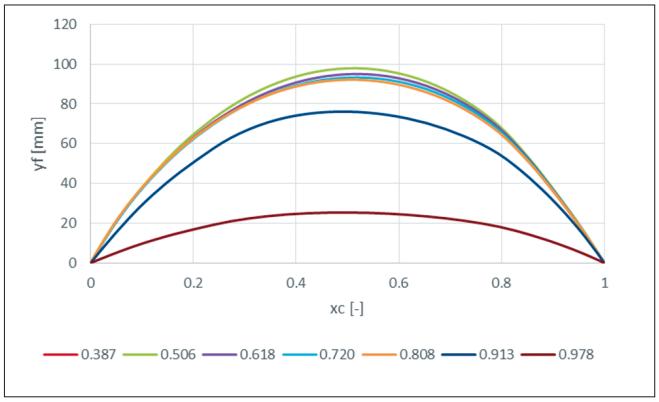

Fig. 8. Wake-adapted propeller P766 mean lines for selected radii, after first iteration (left) and final iteration (right)

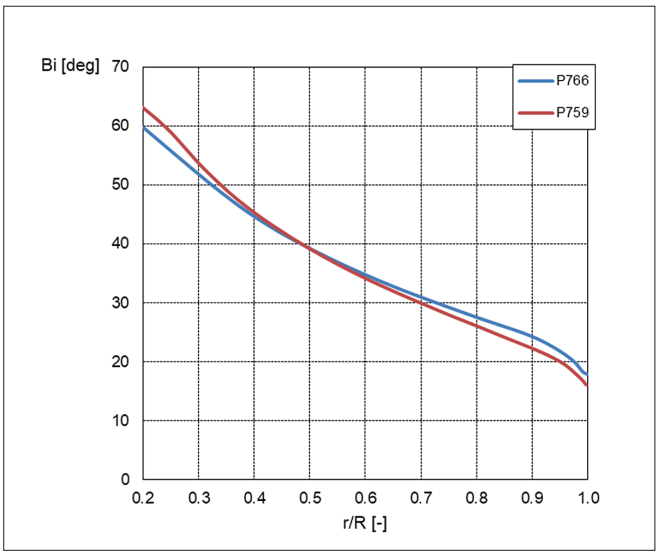

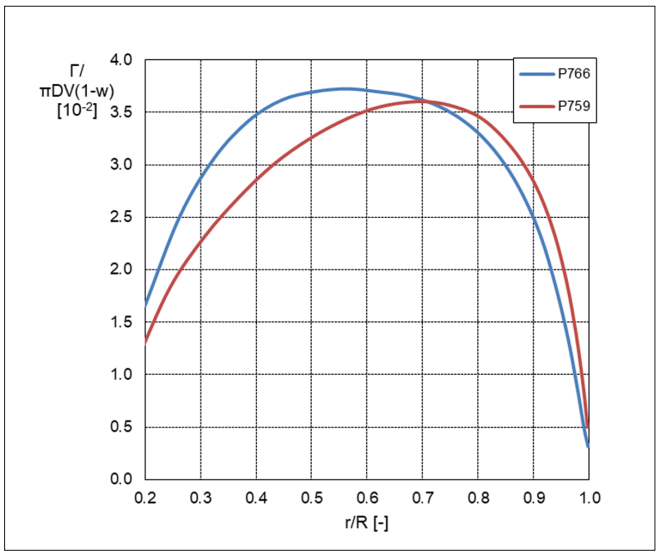

Fig. 9. Induced advance angle (left) and non-dimensional bound circulation (right) distributions

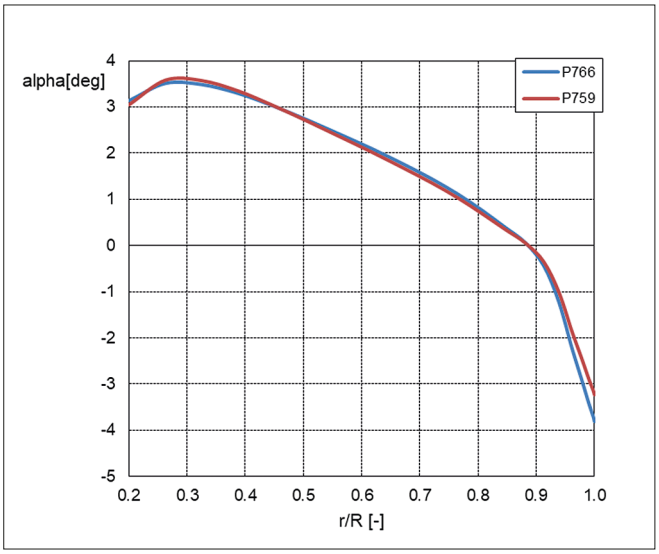

Fig. 10. Angle of attack distributions

Both propellers were subject to open water and self-propulsion tests. All tests were conducted in the CTO Ship Hydromechanics Division at a scale ratio of $\lambda = 30.4502$. Lifting surface calculations were conducted to evaluate the propellers' hydrodynamic properties at their design points. In the case of propeller P759, the comparison of numerical and experimental results is as follows:

Tab. 1. P759 – numerical and experimental results

Case	J	K_T	K_Q
Calculations	0.8839	0.2793	0.0579
Experiment		0.2829	0.0601

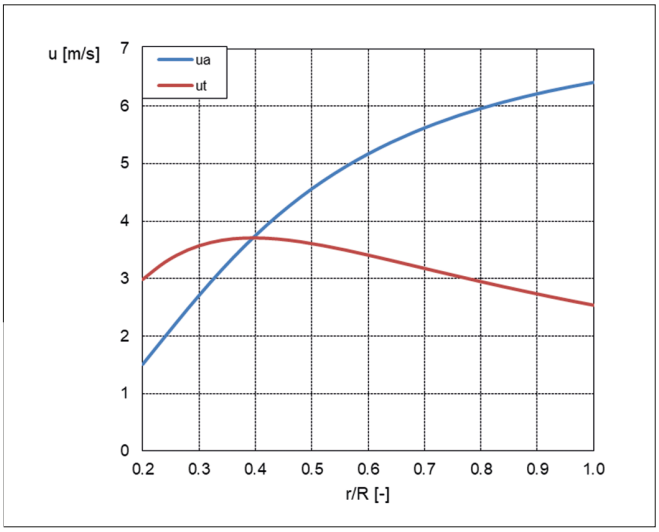

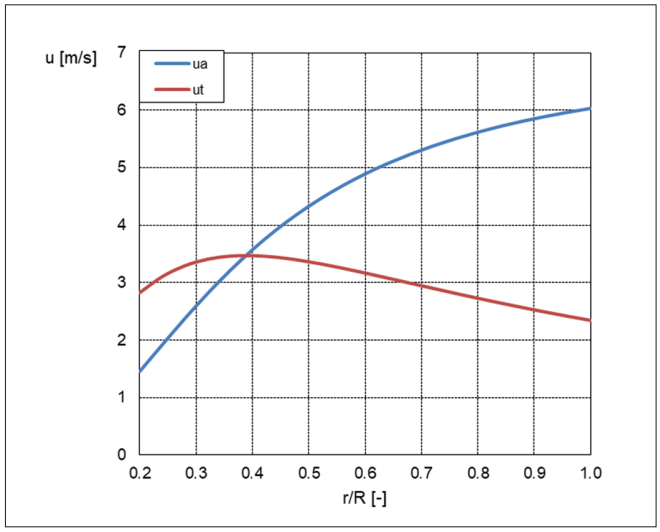

Fig. 11. Induced velocity distributions, P759 (left) and P766 (right)

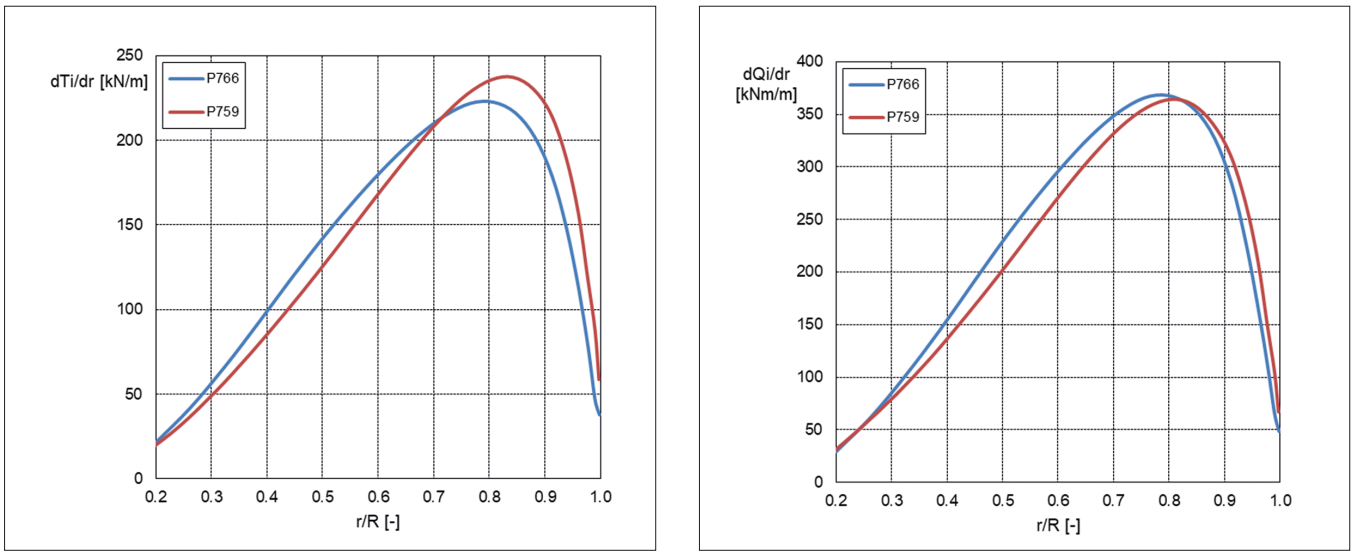

Fig. 12. Inviscid thrust (left) and torque (right) distributions

As the propeller P759 was chronologically the first one, the relation between its numerical and empirical characteristics was utilised to correct the results of the numerical calculations for propeller P766, by altering the calculated KT and KQ values times correction factor α, which is defined as:

$$\alpha = \frac{K_{T/Q\_exp}}{K_{T/Q\_num}} \tag{7}$$

The following results were produced for P766:

Tab. 2. P766 – numerical and experimental results

Case	J	K_T	K_Q
Calculations	0.8979	0.2965	0.0639
Calculations corrected		0.3004	0.0664
Experiment		0.2979	0.0666

The basic measure of blade design correctness is agreement between the assumed rate of revolution at the design point and the obtained value. In this frame, it can be stated that propeller P766 was designed with full success.

Tab. 3. Results of self-propulsion test, rate of revolution

Case	Assumed	P759	P766
n [rpm]	80.0	81.6	79.7

CONCLUSIONS

The lifting surface model forms a reliable basis for designing blade section profiles and screw propeller blades. The approach described in this paper may be utilised also for axial turbines, after slight modifications, and other rotating machinery consisting of lifting blades.

The incorporation of vortex wake deformation allows the propeller pitch distribution to be obtained and adjusted to local inflow conditions.

The simplification applied in the presented design approach, to neglect the radial component of induced velocity, results in a relatively simple and stable algorithm that is nevertheless still capable of providing reliable results.

Further work should reveal the possibility of applying the lifting surface model for designing more complex propulsor systems like a propeller with a guide vane or tandem propellers.

ACKNOWLEDGEMENT

The paper has been elaborated within the frames of the Ship Design and Research Centre's own research program in 2018.

REFERENCES

1. Bugalski T., Streckwall H., Szantyr J. A. (2013): *Critical review of propeller performance scaling methods, based on model experiments and numerical calculations*. Polish Maritime Research, 4(80), Vol. 20, 71–80.

2. Brockett T. (1981): *Lifting-Surface Hydrodynamics for Design of Rotating Blades*, Propellers '81 Symposium.

3. Gaggero S., Gonzalez-Adalid J., Perez Sobrino M. (2016): *Design of contracted and tip loaded propellers by using boundary element methods and optimization algorithms*. Applied Ocean Research, Vol. 55, 102–129.

4. Greeley D. S., Kerwin J. E. (1982): *Numerical methods for propeller design and analysis in steady flow.* SNAME Transactions, Vol. 90, 415–453.

5. Jarzyna H., Koronowicz T., Szantyr J. A. (1996): *Design of marine propellers, Selected problems.* Ossolineum, Wrocław.

6. Kobyliński L. (1955): *Śruby okrętowe (in Polish).* Wydawnictwo Komunikacyjne, Warszawa.

7. Koyama K. (1993): *Comparative calculations of propellers by surface panel method, Workshop organized by 20th ITTC Propulsor Committee.* Papers of Ship Research Institute.

8. Król P., Bugalski T. (2018): *Application of vortex flow model in propeller – stator system design and analysis.* Polish Maritime Research, 1(97), Vol. 25, 35–44.

9. Król P., Tesch K. (2018): *Experimental and numerical validation of the improved vortex method applied to CP745 marine propeller model.* Polish Maritime Research, 2(98), Vol. 25, 57–66.

10. Lee K. J., Hoshino T., Lee J. H. (2014): *A lifting surface optimization method for the design of marine propeller blades.* Ocean Engineering, Vol. 88, 472–470.

11. Lee T., Park S. O. (2009): *Improved iteration algorithm for nonlinear vortex lattice method.* Journal of Aircraft, Vol. 46, No. 6.

12. Luca G., Roberto M., Claudio T. (2014): *Marine propellers performance and flow-field prediction by a free-wake panel method.* Journal of Hydrodynamics, Vol. 26 (5), 780–795.

13. Miclea-Bleiziffer M., Untaroiu A., Delgado A. (2014): *Development of a novel design method for marine propellers by computing the exact lift of arbitrary hydrofoils in cascade.* Ocean Engineering, Vol. 83, 87–98.

14. Morgan B., Silovic V., Denny S. B. (1968): *Propeller Lifting-Surface Corrections.* SNAME Transactions, Vol. 76, 309–347.

15. Muscari R., Mascio A., Verzicco R. (2013): *Modeling of vortex dynamics in the wake of a marine propeller.* Computers & Fluids, Vol. 73, 65–79.

16. Noosomton J., Gunnuang W. (2017): *Case study on CFD simulation and experiment of new developed propeller for training Thai boat.* Fifth International Symposium on Marine Propulsors – SMP'17, Espoo.

17. Suchecki W. (2018): *Studies on velocity fields around the cavitation vortices generated by the model of a rotating blade.* Polish Maritime Research, 2(98), Vol. 25, 66–70.

18. Szantyr J. (1984): *Deformable lifting surface method for determination of unsteady cavitation on screw propeller blade and its hydrodynamic results (in Polish).* IMP PAN Gdańsk.

19. Zeraatgar H., Hossein Ghaemi M. (2019): *The analysis of overall ship fuel consumption in acceleration manoeuvre using hull-propeller-engine interaction principles and governor features.* Polish Maritime Research, 1(101), Vol. 26, 162–173.

CONTACT WITH THE AUTHORS

Przemysław Król
e-mail: krolprz30@gmail.com

Ship Design and Research Centre
Szczecińska 65, 80-392 Gdańsk

Gdańsk University of Technology
Gabriela Narutowicza, 80-233 Gdańsk,
Poland